Proc. Natl. Acad. Sci. USA
Vol. 92, pp. 12120–12125, December 1995
Biochemistry

This contribution is part of the special series of Inaugural Articles by members of the National Academy of Sciences elected on April 25, 1995.

Active site topology and reaction mechanism of GTP cyclohydrolase I

HERBERT NAR§¶, ROBERT HUBER§, GÜNTER AUERBACH§, MARKUS FISCHER‖, CORNELIA HÖSL‖, HARALD RITZ‖, ANDREAS BRACHER‖, WINFRIED MEINING‖, SABINE EBERHARDT‖, AND ADELBERT BACHER‖

§Max-Planck-Institut für Biochemie, Am Klopferspitz, D-82152 Martinsried, Federal Republic of Germany; and ‖Institut für Organische Chemie und Biochemie, Technische Universität München, Lichtenbergstrasse 4, D-85747 Garching, Federal Republic of Germany

Contributed by Robert Huber, October 13, 1995

ABSTRACT **GTP cyclohydrolase I of *Escherichia coli* is a torus-shaped homodecamer with D_5 symmetry and catalyzes a complex ring expansion reaction conducive to the formation of dihydroneopterin triphosphate from GTP. The x-ray structure of a complex of the enzyme with the substrate analog, dGTP, bound at the active site was determined at a resolution of 3 Å. In the decamer, 10 equivalent active sites are present, each of which contains a 10-Å deep pocket formed by surface areas of 3 adjacent subunits. The substrate forms a complex hydrogen bond network with the protein. Active site residues were modified by site-directed mutagenesis, and enzyme activities of the mutant proteins were measured. On this basis, a mechanism of the enzyme-catalyzed reaction is proposed. Cleavage of the imidazole ring is initiated by protonation of N7 by His-179 followed by the attack of water at C8 of the purine system. Cystine Cys-110 Cys-181 may be involved in this reaction step. Opening of the imidazole ring may be in concert with cleavage of the furanose ring to generate a Schiff's base from the glycoside. The γ-phosphate of GTP may be involved in the subsequent Amadori rearrangement of the carbohydrate side chain by activating the hydroxyl group of Ser-135.**

GTP cyclohydrolase I (CYH) catalyzes a ring expansion conducive to the formation of dihydroneopterin triphosphate (compound **4**) from GTP (compound **1**) (Fig. 1). It has been proposed that the reaction is initiated by opening of the imidazole ring of compound **1.** Intermediate **2** could then undergo an Amadori rearrangement yielding compound **3**, which could subsequently undergo ring closure to yield the product **4** (for review, see ref. 1). This reaction is the first committed step of several biosynthetic pathways. Thus, the enzyme product serves as the precursor of tetrahydrofolate in eubacteria, fungi, and plants and of the folate analogs of methanogenic bacteria (1, 4). In vertebrates and insects (5), compound **4** is the biosynthetic precursor of tetrahydrobiopterin, which is involved in the formation of catecholamines and nitric oxide (6, 7). Tetrahydrobiopterin is also involved in the stimulation of T lymphocytes, although the details are still incompletely understood (8).

CYH was originally detected in bacteria (9). More recently, the primary structure of CYH from a wide variety of organisms has been determined (10–16). The evolution of the protein has been relatively conservative. Thus, the C-terminal 120 residues of *Escherichia coli* and human enzymes are 60% identical. The crystal structure of *E. coli* CYH has recently been solved by single isomorphous replacement and averaging techniques

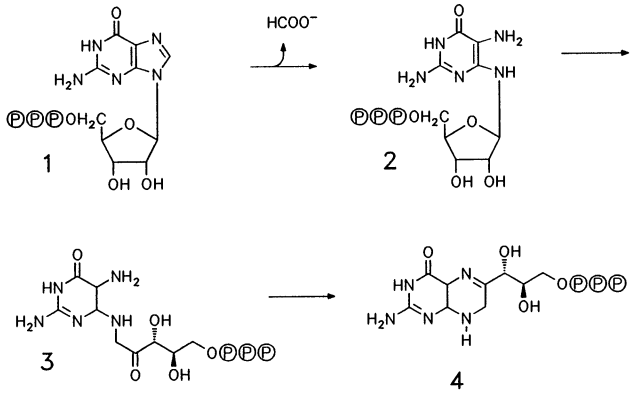

FIG. 1. Basic steps in the reaction mechanism of CYH as proposed by Brown and coworkers (1–3).

(17). The knowledge of the crystal packing arrangement obtained by electron microscopy (18, 19) was helpful in the initial stages of structure determination. The enzyme complex, a decamer consisting of a pentamer of tightly associated dimers, is doughnut shaped with dimensions of 65 × 100 Å.

One CYH subunit folds into a α+β structure with a predominantly helical N terminus (Fig. 2). The N-terminal helix h1 (residues 5–18) is followed by a helix pair, composed of helix h2 (residues 32–49) and helix h3 (residues 62–72), which are remote from the compact C-terminal domain of the molecule (residues 95–217). This domain has a central four-stranded antiparallel β-sheet that is flanked on both sides by α-helices. The folding topology of this domain is identical to that of a subunit of the second enzyme in tetrahydrobiopterin biosynthesis pathway, 6-pyruvoyltetrahydropterin synthase (20).

The association of two CYH monomers to dimers is driven by the formation of a four-helix bundle by helices h2 and h3 of each monomer. Apart from a large hydrophobic surface buried by this interaction, numerous hydrogen bonds and salt bridges serve to stabilize the dimer. The decamer is formed by a fivefold symmetric arrangement of the dimers. Its most striking structural feature is an unprecedented 20-stranded antiparallel β-barrel (Fig. 2).

This paper describes the crystal structure of a complex of CYH with dGTP, the substrate analog.** By using the infor-

The publication costs of this article were defrayed in part by page charge payment. This article must therefore be hereby marked "*advertisement*" in accordance with 18 U.S.C. §1734 solely to indicate this fact.

Abbreviation: CYH, GTP cyclohydrolase I.

¶Present address: Karl Thomae GmbH, Structural Research, Birkendorferstrasse 65, D-88397 Biberach, Federal Republic of Germany.

**The atomic coordinates have been deposited in the Protein Data Bank, Chemistry Department, Brookhaven National Laboratory, Upton, NY 11973 (code 1GTP).

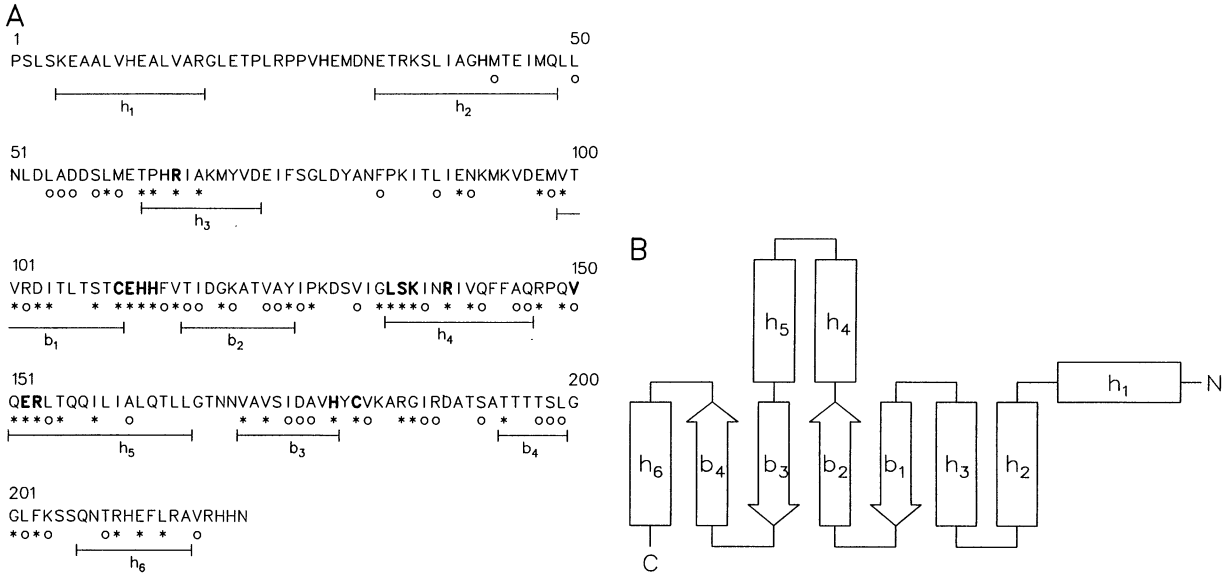

FIG. 2. (*A*) Sequence of CYH of *E. coli*. Absolutely conserved residues are indicated by asterisks, and conservative residues are indicated by circles. Residues subjected to mutagenesis in this study are shown in boldface type. (*B*) Schematic representation of the folding pattern. h, Helix; b, β-sheet.

mation of the spatial structure of the dGTP complex and kinetic analyses of a variety of active site mutants, we propose a reaction scheme for the complex organic chemistry catalyzed by CYH.

EXPERIMENTAL PROCEDURES

Construction of the FolE Expression Clone. The gene for CYH of *E. coli* was inserted into a slightly modified derivative of the expression vector pDS56/RBSII,NcoI (21). The 5′ end of the gene was reconstructed by using a synthetic linker. The gene is under control of a *lac* operator and T5 promoter.

Site-Directed Mutagenesis. Active site mutagenesis was performed by PCR strategies to be published elsewhere. All constructs were verified by DNA sequencing using a Perkin–Elmer/Applied Biosystems Prism 377 DNA sequencer.

Protein Purification. A frozen cell mass (3 g) was thawed in 12 ml of 0.2 M Tris·HCl (pH 8) containing 2.5 mM EDTA, 1 mM phenylmethylsulfonyl fluoride, 18 mg of lysozyme, and 0.54 mg of DNase. The mixture was incubated at 37°C for 90 min. The suspension was centrifuged, and the supernatant was dialyzed against 2 liters of 10 mM sodium phosphate (pH 7.0) containing 2.5 mM EDTA and 0.3 mM sodium azide. The solution was placed on a column of DEAE-cellulose DE 52 (5 × 1 cm) that had been equilibrated with 10 mM sodium phosphate (pH 7.0) containing 2.5 mM EDTA. The column was developed with a linear gradient of 10–150 mM sodium phosphate (pH 7.0). Fractions were collected and concentrated by ultracentrifugation.

Assay for CYH Activity. Assay mixtures contained 100 mM Tris·HCl (pH 8.5) containing 0.1 M KCl, 2.5 mM EDTA, 310 μM GTP, and protein. The mixtures were incubated at 37°C. Aliquots of 100 μl were retrieved at intervals, and the enzyme reaction was terminated by the addition of 12 μl of 1 M HCl containing 1% I_2 and 2% (wt/vol) KI. The samples were incubated at room temperature for 10 min. A solution of 2% (wt/vol) ascorbate (6 μl) was added to reduce the excess of iodine. NaOH (1 M, 16 μl) was added, followed by the addition of 10 μg of alkaline phosphatase dissolved in 6 μl of 50 mM $MgCl_2$ containing 65 mM $ZnCl_2$. The mixture was incubated at 37°C for 15 min, and 60 μl of 40% (wt/vol) trichloroacetic acid was added. The samples were analyzed by reversed-phase HPLC using a column of Nucleosil RP18 (4 × 250 mm) and an eluent containing 30 mM HCOOH and 7% MeOH. Neo-

Table 1. Crystallographic data

	NATI1	NATI2	$dGTP_{complete}$ (90 × 0.8°)	$dGTP_{partial}$ (30 × 0.8°)
Source	RA	DESY	RA	RA
Observations, no.	383,603	396,136	263,212	94,758
Unique reflections, no.	76,754	126,898	86,912	65,107
R_{merge}, %	11.0	5.3	13.2	13.4
Resolution, Å	3.2	2.6	3.0	3.0
Data completeness, %	99.4	91.7	91.2	69.4
No. of atoms in refinement		26,295	26,445	
Resolution range, Å		8–2.6	8–3.0	
No. of reflections used		122,703	82,450	
B_{aver}, Å^2		32.0	31.9	
R factor, %		20.8	24.9	
R free, %		27.0	—	
rms bond, Å		0.008	0.007	
rms angles, degrees		1.83	2.13	
rms deviation between monomers, Å		0.22	0.04	
rms bonded *B*, Å^2		4.66	4.75	

RA, rotating anode source; DESY, Deutsche Elektronin Synchrotion source.

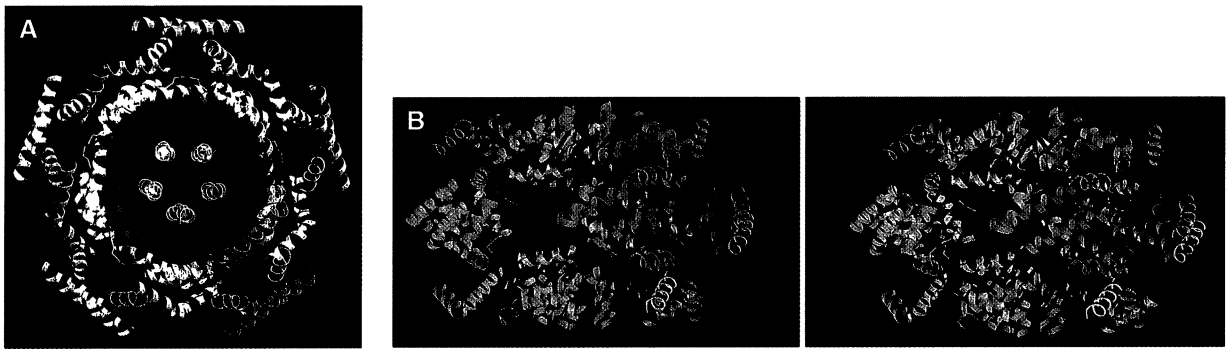

FIG. 3. Ribbon representation of a CYH decamer. Helices, yellow; β-strands, red; turns, blue. (*A*) View along the molecular fivefold symmetry axis. The core of the active enzyme complex is formed by a 20-stranded antiparallel β-barrel surrounding five α-helices. The periphery of the decamer is predominantly helical. (*B*) Stereo view of the decamer perpendicular to the fivefold axis.

pterin was detected fluorometrically (excitation, 365 nm; emission, 446 nm).

Immunodiffusion. Radial immunodiffusion was performed in 0.56% agarose gel containing 100 mM potassium phosphate (pH 7.0) and 100 μl of anti-CYH serum from rabbit (22). The plates were incubated at 37°C overnight. Wild-type CYH was used as standard. Two-dimensional double-diffusion experiments were performed with 0.56% agarose gels containing 100 mM potassium phosphate (pH 7.0) (22).

Crystallization. Crystals of CYH were obtained under a variety of conditions (23, 24). The crystal modification used for the present study was obtained by vapor diffusion. A solution containing CYH at 10 mg/ml was mixed with an aliquot of precipitant solution and the mixture was equilibrated against a reservoir containing either 6% (wt/vol) PEG (M_r = 6000), 0.1 M $(NH_4)_2SO_4$, and 0.1 M Mops (pH 7) (buffer 1) or 0.2 M sodium acetate and 0.1 M Mes (pH 6) (buffer 2). Both precipitants produced a C-centered, orthorhombic crystal form with unit-cell dimensions of a = 315.0 Å, b = 227.2 Å, and c = 131.5 Å and a space group of $C222_1$. If there are 12 CYH decamers per unit cell, the packing constant is calculated as V_m = 3.2 Å^3/Da, suggesting that at least one CYH decamer is located on a diad axis.

Data Collection and Structure Solution. Reflection data were collected from crystals grown from buffer 1 on MAR imaging plates (MAR Research, Hamburg, Germany), processed with MOSFLM (25), and reduced with programs of the CCP4 package. First native data to 3.2-Å resolution were obtained by using a rotating anode Cu-K_α radiation source. The resolution was then extended to 2.6 Å by using synchrotron radiation (Table 1).

The structure was solved by Patterson search techniques using AMORE (26). As the search model, we used a CYH pentamer from the refined structure of *E. coli* CYH crystallized in the monoclinic space group $P2_1$ (17). Rotation and translation functions (resolution of 8–4 Å, data set NATI1) yielded clear signals for three pentamers per asymmetric unit. After rigid body refinement, the correlation coefficient was 60.6%, and the R factor was 42.9%. As anticipated, one pentamer was placed close to a crystallographic diad parallel to b at x = ½, y = ¼, and z = ¼. Refinement proceeded in several steps of model rebuilding, positional and temperature factor refinement, with O (27) and XPLOR (28), using the high-resolution synchrotron data (NATI2), whereby care was taken to keep the model close to ideal stereochemistry with strong restraints on noncrystallographically related atomic positions and B factors.

Complex with dGTP. The structure of CYH obtained as above contains a XO_4 anion bound to a cluster of basic residues close to the active site of each monomer. Since both orthophosphate (10 mM in the protein buffer solution) and sulfate (100 mM in the precipitant buffer) are present during crystallization, an unambiguous identification of the nature of the anion was not possible. However, for a complexation experiment with dGTP, the substrate analog, we wished to prevent competition for the binding site between ions present in the mother liquor and the added inhibitor. Therefore, for the soaking experiment, we chose to work with crystal specimens that are isomorphous to those used above but were grown from buffer 2. Soaking with a stabilizing solution (0.4 M sodium acetate/0.1 M Mes, pH 6) containing 10 mM dGTP was performed for 90 min, followed by data collection (Table 1). The final model of the native structure was refined against the complex data and used to calculate a ΔF electron density. Fifteenfold noncrystallographic symmetry averaging with MAIN (29) was used to improve the signal of the difference map.

RESULTS AND DISCUSSION

Structure of the dGTP Complex. Ribbon diagrams of CYH viewed along the fivefold axis and perpendicular to the fivefold

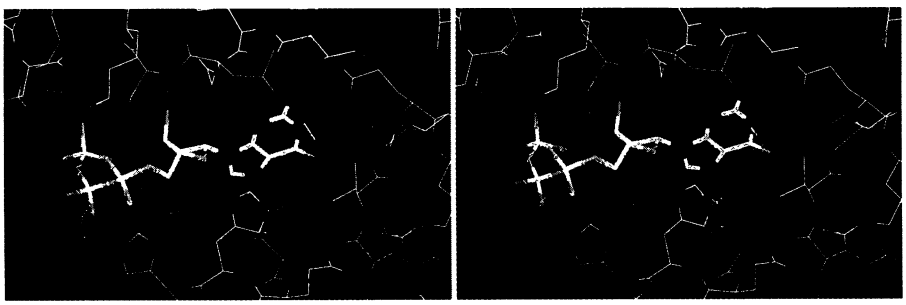

FIG. 4. Stereo view of the atomic structure of the active site of CYH harboring dGTP. The fifteenfold averaged $F_O - F_C$ electron density map (computed with data set $dGTP_{partial}$ contoured at 6σ) is shown in blue. It clearly indicates the position of the triphosphate, the ribose, and guanine moieties. The missing density for the C8 atom and the additional density close to the Cys-110 side chain suggest partial conversion via imidazole hydrolysis.

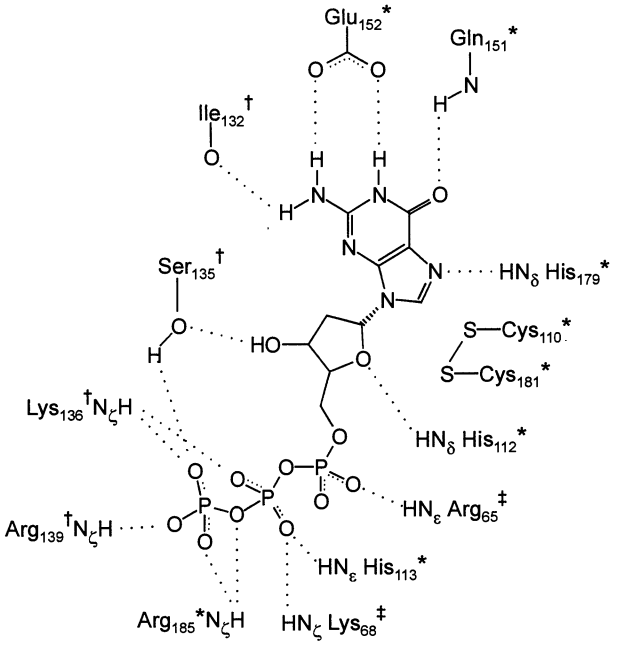

FIG. 5. Schematic representation of the interactions of active site residues with dGTP. Residues are labeled *, †, and ‡ to indicate their origin at three different CYH monomers. All residues involved in dGTP binding are highly conserved, except Lys-68, which is replaced by Ser and Thr in some sequences.

axis are shown in Fig. 3. They show the overall topology of the catalytically active decamer.

To unequivocally locate the active sites within the decamer, an orthorhombic crystal of CYH soaked with 10 mM dGTP was used for x-ray analysis. The difference electron density

Table 2. Relative specific activities of CYH mutants

Protein	Relative specific activity, %
Wild type	100*
R65A	3.0
C110S	≤0.02*
E111A	≤0.93
E111D	25
E111Q	1.0
H112D	≤0.04
H112F	≤0.04
H112R	≤0.04
H112S	≤0.04
H113F	≤0.2
H113S	≤0.07*
L134S	3.9
S135W	≤0.3
K136G	5.7
R139A	52*
V150T	64
E152D	≤0.07*
E152Q	≤0.1
R153A	88
H179F	≤0.6
C181A	≤0.04
C181S	≤0.07*

Expression plasmids carrying copies of mutated genes were expressed in *E. coli*. Mutant proteins indicated by asterisks were purified to homogeneity. Other enzyme activities were estimated from experiments with crude cell extracts where the concentration of CYH was estimated by radial immunodiffusion. The host strain carried a chromosomal copy of the wild-type CYH gene, and small amounts of wild-type enzyme were, therefore, present in all cell extracts.

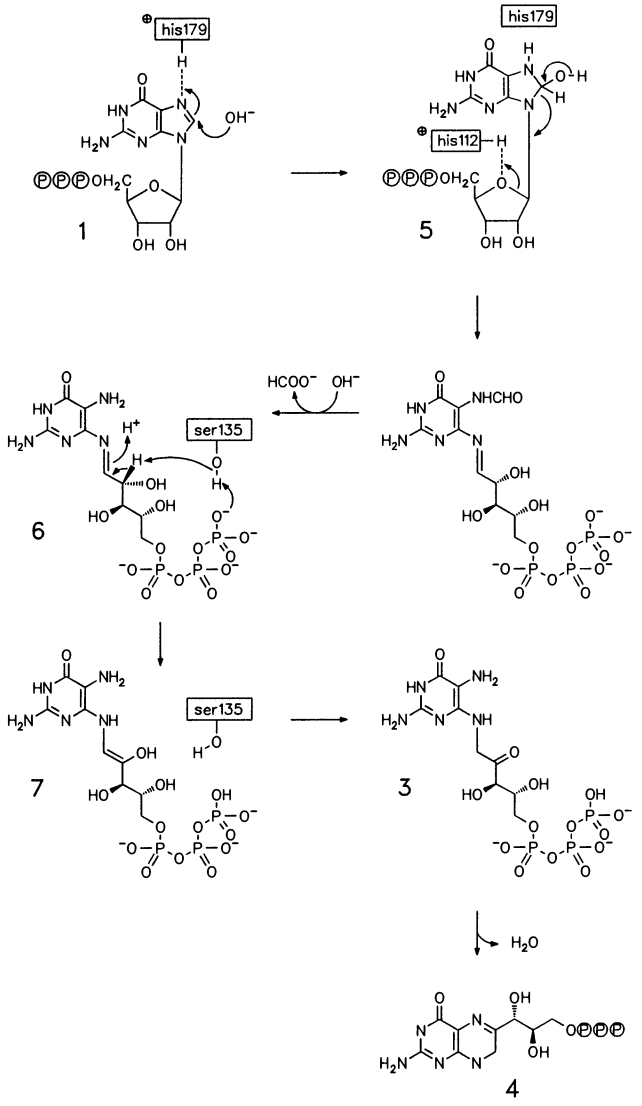

FIG. 6. Hypothetical mechanism for CYH proposed on basis of crystallographic and mutagenesis data.

map of the dGTP complex (Fig. 4) shows clearly how the substrate analog is bound to the enzyme. The active site of CYH is located at the interface of three subunits (two from one pentamer and one from the other pentamer; the corresponding subunit residues are labeled by *, †, or ‡ superscripts hereafter). Due to the 52-point group symmetry of the homodecameric enzyme complex, there are 10 equivalent active sites per functional unit. The protein acceptor site for the substrate analog contains a 10-Å-deep pocket that seems ideally suited to receive the nucleoside triphosphate molecule. The three sequentially distant loop segments of residues 109*–113*, 150*–153*, and 179*–181* on the first subunit form the major part of the active site cavity. The loops are structurally stabilized by extensive short-range hydrogen bond interactions and are, furthermore, mutually linked by the disulfide bridge Cys-110* Cys-181*, the salt bridge Glu-111*–Arg-153*, and the hydrogen bond interaction Gln-151*–His-179*. This results in a strictly confined conformational space available to residues involved in substrate recognition and catalysis.

The protein acceptor site for the pyrimidine portion of the purine ring system is found at the bottom of the active site cavity. Glu-152* forms a salt bridge with the guanidine moiety. The preceding peptide bond between Val-150* and Gln-151* forms a hydrogen bond with its amide hydrogen to the C-4 oxo group of the purine. Further, a hydrogen bond is formed

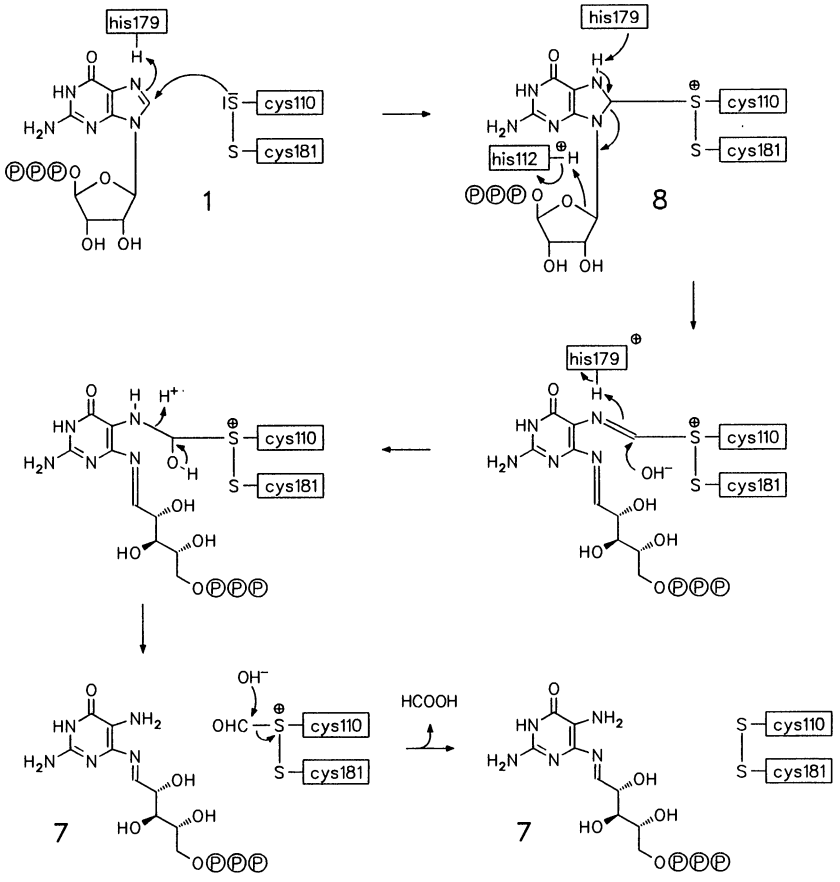

FIG. 7. Alternative hypothetical mechanism for opening of the imidazole ring.

between the N-2 of the nucleobase and the carbonyl oxygen of residue Ile-132† (Fig. 5). This peculiar recognition pattern is specific for guanine and explains the selectivity of the enzyme for GTP over ATP (30). The inner wall of the pocket that lies parallel to the pyrimidine ring plane is lined by residues Val-150* and Leu-134† that create a suitably hydrophobic environment. The imidazole portion of the nucleobase is flanked by the cystine Cys-110* Cys-181* and is hydrogen bonded to His-179*. There is space left on both sides of its ring plane that might be occupied by solvent during catalysis.

A cluster of basic residues, His-113*, Arg-185*, Lys-136†, Arg-139†, Arg-65‡, and Lys-68‡, at the pocket entrance binds the triphosphate group of the dGTP. Since these residues provide for complete charge compensation, Mg^{2+} assisted binding to the protein, as found in other nucleoside triphosphate binding proteins, is neither necessary nor realized in CYH.

The electron density for the carbohydrate part of dGTP is less well defined than for the rest of the molecule when using a complete crystallographic data set for map calculation that averages ≈48 h of data collection time (Table 1; data set dGTP complete). When we used the crystallographic data measured in the first 10 h after soaking (Table 1; data set dGTP partial), we obtained a well-defined $F_O - F_C$ density for the deoxyribose in its furanose form (Fig. 4). This suggests that dGTP is processed very slowly in the CYH crystals and that the reaction probably involves ribose ring opening. Preliminary chemical evidence for dGTP conversion by CYH to 2,5-diamino-6-(2′-deoxyribosylamino)-4(3H)-pyrimidinedione 5′-triphosphate was obtained by using an enzyme assay developed for GTP cyclohydrolase II (31). The room temperature reaction rate seems to be slow even on the crystallographic time scale, in accordance with the x-ray data.

The deoxyribose moiety is positioned such that its ring oxygen atom is hydrogen bonded to His-112*, which in turn is held in position by a hydrogen bond network on the other side of its imidazole ring (Glu-111* O^{ε} ... Ser-58‡ $O^{\gamma}H$ ... His-112* N^{ε}) even in the absence of substrate or analog. Ser-135† is in hydrogen bond distance with its side-chain hydroxyl functional group to the 3′-hydroxyl of dGTP. Since the ribose triphosphate is bound to the enzyme in an unusual bent conformation, the Ser side chain is also hydrogen bonded to the γ-phosphate of the substrate analog.

Functional Groups Involved in Enzyme Catalysis. The amino acid residues lining the active site cavity of GTP cyclohydrolase are well defined by the reported x-ray data. To define more clearly the functional significance of individual residues, a large number of mutants were obtained by site-directed mutagenesis of a hyperexpression plasmid directing the synthesis of CYH (Table 2).

The hyperexpression plasmid and the mutant plasmids are conducive to the formation of ≈30% CYH, based on total cell protein as shown by polyacrylamide gel electrophoresis and by radial immunodiffusion. All mutant proteins shown in Table 2 gave complete cross reaction with the wild-type protein in double immunodiffusion experiments with a rabbit antiserum against wild-type *E. coli* CYH. The crude cell extracts of the recombinant mutant strains were assayed for enzyme activity, and the concentration of mutant CYH was estimated by radial immunodiffusion. Some of the mutant proteins were purified to homogeneity.

The host strain carries a chromosomal copy of the wild-type gene for CYH, and small amounts of the wild-type protein were thus present in all cell extracts. As a consequence, some enzyme activity would be observed even with a totally inactive mutant. On this basis, the structure–activity relationship of individual amino acid residues can be described as follows.

The binding of the nucleobase deep in the active site pocket places the imidazole ring proton at C-8 in close proximity to the disulfide bridge Cys-110* Cys-181*, which forms the central part of the active site structure. The distance between the Cys-110* S^{γ} and the C-8 is 3.5 Å. Site-directed mutagenesis experiments show that the elimination of the disulfide bridge by replacement of either of the Cys residues with Ala or Ser results in a virtually complete loss of enzyme activity (Table 2).

The purine hydrolysis reaction could be initiated by protonation of the nucleobase at N-7 by His-179*. Replacement of His-179 by Phe results in a loss of catalytic activity (Table 2). The positive charge on the imidazole renders the C-8 atom prone to nucleophilic attack. A water molecule could then act as the nucleophile that initiates the imidazole ring cleavage (Fig. 6). It has been shown earlier that 7,9-disubstituted purines can undergo a nonenzymatic ring opening reaction under mild alkaline conditions (32). Hydration of GTP protonated at N-7 would yield the intermediate **5.** The opening of the imidazole ring could then be assisted by protonation of the bridging O atom in the furanose by His-112. The furanose ring and the imidazole ring could then both be opened in a concerted reaction yielding the Schiff's base intermediate **6.** In line with this hypothesis, the exchange of His-112 for Phe yields enzyme of very low activity.

Alternatively, the cystine might be the agent that attacks the C-8 of the purine (Fig. 7). Nucleophilic attack of C-8 of the purine by the sulfur of Cys-110 would involve the formation of a thiasulfonium ion intermediate **8** (33) that would react with solvent to restore the cystine. However, no precedent for this hypothetical reaction sequence is known as yet.

The Amadori rearrangement of intermediate **6** probably involves the loss of the C-2′ proton and keto–enol tautomerization to yield the C-1′ methylene, C-2′ keto intermediate **3.** On the basis of the dGTP complex structure, we propose that Ser-135† acts as the base for C-2′ proton abstraction. It is located in close proximity to the C-2′–C-3′ bond of the sugar. In the case of the dGTP complex, the structure suggests a hydrogen bond between Ser-135 and the 3′ hydroxyl group of the substrate. In case of GTP, the natural substrate, a slight reorientation of the carbohydrate moiety could bring Ser-135 into the correct position for abstraction of the 2′ hydrogen atom. The basicity of Ser-135 is probably increased by the interaction with the γ-phosphate of GTP (Fig. 6). The suggestion of substrate induced activation of the functional group of the enzyme is supported by the fact that neither GDP nor GMP act as substrate for CYH (2).

The last reaction step is the formation of a Schiff's base between the C-2′ carbonyl and the N-7 amine group conducive to ring closure. The product dihydroneopterin triphosphate (**4**) could be formed in the active site of the enzyme. However, the spatial structure of the active site suggests that the side chain at the C6 position of the pterin ring system would lie close to and point into the direction of the loop between residues 110* and 113*, given an unchanged position of the pyrimidine moiety of substrate and product. Therefore, we assume that either the ring closure takes place at the protein surface, after a considerable reorientation of the heterocycle or, in solution, after dissociation of the intermediate from the enzyme.

We thank Dr. H. D. Bartunik for assistance during crystallographic data collection at the BW6 beamline at DESY and Profs. P. Boyle and C. Suckling for stimulating discussions. We also thank Angelika Kohnle for expert help with the preparation of the manuscript. This work was supported in part by grants from the Deutsche Forschungsgemeinschaft, the European Community (Contract ERBCHRXCT930166 and ERBCHRXCT930243), and the Fonds der Chemischen Industrie.

1. Brown, G. M. & Williamson, J. M. (1987) in *Escherichia coli and Salmonella typhimurium*, ed. Neidhardt, F. C. (Am. Soc. Microbiol., Washington, DC), Vol. 1, pp. 521–538.
2. Yim, J. J. & Brown, G. M. (1976) *J. Biol. Chem.* **251,** 5087–5094.
3. Wolf, W. A. & Brown, G. M. (1969) *Biochim. Biophys. Acta* **192,** 468–478.
4. Eisenreich, W. & Bacher, A. (1994) *Pteridines* **5,** 8–17.
5. Nichol, C. A., Smith, G. K. & Duch, D. S. (1985) *Annu. Rev. Biochem.* **54,** 729–764.
6. Tayeh, M. A. & Marletta, M. A. (1989) *J. Biol. Chem.* **264,** 19654–19658.
7. Kwon, N. S., Nathan, C. F. & Stuehr, D. J. (1989) *J. Biol. Chem.* **264,** 20496–20501.
8. Ziegler, I. (1990) *Med. Res. Rev.* **10,** 95–114.
9. Burg, A. W. & Brown, G. M. (1966) *Biochim. Biophys. Acta* **117,** 275–278.
10. Hatakeyama, K., Inoue, Y., Harada, T. & Kagamiyama, H. (1991) *J. Biol. Chem.* **266,** 765–769.
11. Katzenmeier, G., Schmid, C., Kellermann, J., Lottspeich, F. & Bacher, A. (1991) *Biol. Chem. Hoppe Seyler* **372,** 991–997.
12. Babitzke, P., Gollnick, P. & Yanofsky, C. (1992) *J. Bacteriol.* **174,** 2059–2064.
13. Togari, A., Ichinose, H., Matsumoto, Sh., Fujita, K. & Nagatsu, T. (1992) *Biochem. Biophys. Res. Commun.* **187,** 359–365.
14. McLean, J. R., Krishnakumar, S. & O'Donnel, J. M. (1993) *J. Biol. Chem.* **268,** 27191–27197.
15. Nomura, T., Ichinose, H., Sumi-Ichinose, C., Nomura, H., Hagino, Y., Fujita, K. & Nagatsu, T. (1993) *Biochem. Biophys. Res. Commun.* **191,** 523–527.
16. Lacks, S. A., Greenberg, B. & Lopez, P. (1995) *J. Bacteriol.* **177,** 66–74.
17. Nar, H., Huber, R., Meining, W., Schmid, C., Weinkauf, S. & Bacher, A. (1995) *Structure* **3,** 459–466.
18. Meining, W., Nar, H., Schmid, C., Bacher, A., Bachmann, L. & Weinkauf, S. (1994) *Pteridines* **5,** 77.
19. Meining, W., Bacher, A., Bachmann, L., Schmid, C., Weinkauf, S., Huber, R. & Nar, H. (1995) *J. Mol. Biol.* **253,** 208–218.
20. Nar, H., Huber, R., Heizmann, C. W., Thöny, B. & Bürgisser, O. (1994) *EMBO J.* **13,** 1255–1262.
21. Stüber, D., Matile, H. & Garotta, G. (1990) *Immunol. Methods* **4,** 121–152.
22. Catty, D. & Raykundalia, C. (1988) in *Antibodies: A Practical Approach*, ed. Catty, D. (IRL, Oxford) Vol. 1, pp. 137–168.
23. Schmid, C., Ladenstein, R., Luecke, H., Huber, R. & Bacher, A. (1992) *J. Mol. Biol.* **226,** 1279–1281.
24. Schmid, C., Meining, W., Weinkauf, S., Bachmann, L., Ritz, H., Eberhardt, S., Gimbel, W., Werner, T., Lahm, H.-W., Nar, H. & Bacher, A. (1993) in *Chemistry and Biology of Pteridines and Folates*, eds. Ayling, J. B., Nair, M. & Baugh, C. M. (Plenum, New York), pp. 157–162.
25. Leslie, A. G. W. (1991) in *Crystallographic Computing V*, eds. Moras, D., Podjarny, A. D. & Thierry, J. C. (Oxford Univ. Press, Oxford), pp. 27–38.
26. Navazza, J. (1994) *Acta Crystallogr. A* **50,** 157–163.
27. Jones, T. A., Bergdall, M. & Kjeldgaard, M. (1990) in *Crystallography and Modelling Methods in Molecular Design*, eds. Bugg, C. & Falick, S. (Springer, New York), pp. 189–199.
28. Brünger, A. T. (1992) XPLOR, A System for X-ray Crystallography and NMR (Yale Univ., New Haven, CT), Version 3.1.
29. Turk, D. (1992) Ph.D. thesis (Technical University, Munich).
30. Burg, A. W. & Brown, G. M. (1968) *J. Biol. Chem.* **243,** 2349–2358.
31. Richter, G., Ritz, H., Katzenmeier, G., Volk, R., Kohnle, A., Lottspeich, F., Allendorf, D. & Bacher, A. (1993) *J. Bacteriol.* **175,** 4045–4051.
32. Fink, K., Adams, W. S. & Pfleiderer, W. (1964) *J. Biol. Chem.* **239,** 4250–4256.
33. Oae, S., Numata, T. & Yoshiaki, Y. (1981) in *The Chemistry of Sulphonium Group*, eds. Stirling, C. J. M. & Patai, S. (Wiley, New York), Part 2, pp. 571–672.